

Image Processing of Mammographic Images using Holography and Interferometry

A.M. Hamed

Physics Department, Faculty of Science, Ain Shams University, Cairo 11566, Egypt.

***Corresponding Author:** A.M. Hamed, Physics Department, Faculty of Science, Ain Shams University, Cairo 11566, Egypt. E- mail: amhamed73@hotmail.com

ABSTRACT

In this paper, improved reconstruction from the coded Fourier hologram of the cancerous mammographic images using Wiener filter is obtained. In addition, image segmentation of the cancerous images using median filter, removal of small objects, and removal of connected objects on the border of the image, are investigated using multiple beam interference. Results and discussion is given followed by a conclusion.

Keywords: Segmentation, mammographic images, Fourier holography, multiple beam interference.

INTRODUCTION

An improved reconstruction from the Fourier hologram using a spatial light modulator (SLM) was investigated. The method is based on applying a digital pre-filtering of the SLM's encoded distribution to compensate the signal distortion caused by the SLM's finite pixel size [1]. Recently, the processing of the plasma images using Fourier holograms is considered in [2-12], where improved reconstructed images are obtained using Wiener filtering.

In the past decades, many applications based on measuring the fringe shift in optical and synthetic fibers in order to get refractive index information [13- 26] are outlined. Recently, digital two and multiple beam interference are applied on Corona virus image and other medical images [27, 28] in order to extract refractive index which is related to the fringe shift. In addition, cascaded two beam interference arrangement giving intensity of higher orders of $\cos^2\theta$ in the form of $\cos^{2n}\theta$, where n represents the number of feedback passes to the interferometer is investigated [29, 30].

In this paper, firstly, an improved reconstructed mammographic images considering Fourier holography are obtained by the filtration as in [12]. The segmented cancerous zones obtained from the reconstructed images are investigated.

Secondly, image processing of the cancerous mammographic images giving interferometric images corresponding to the segmented cancer are investigated.

THEORETICAL ANALYSIS

The mammographic image is recorded numerically as a Fourier hologram using Mat Lab code as follows: Firstly, a diffuser of the same dimensions like the rescaled gray scale image of dimensions 512×512 pixels is constructed numerically. Secondly, the multiplication of both the cancerous mammographic image and the diffuser is Fourier transformed numerically to get the holographic interference image. It is represented by the convolution product of the Fourier transform of the mammographic image and the speckle pattern. It is noted that the speckle pattern is computed by operating the Fourier transform upon the diffuser. Thirdly, the inverse Fourier transform is operated upon the described Fourier hologram to get the reconstructed cancerous mammographic images.

The two Fourier transform operations are summarized as follows:

1st step: Recording of the amplitude and the phase of the hologram

The complex amplitude of the image is analytically represented as:

$$A(x, y) = a(x, y) \exp[j\Phi(x, y)] \quad (1)$$

It is numerically written as follows:

$$A(x, y; \lambda) = \sum_{n=1}^N \sum_{m=1}^M a(m \Delta x, n \Delta y) \exp[j \Phi(m \Delta x, n \Delta y; \lambda_i)] \quad (2)$$

Where the continuous variables (x, y) are replaced by numerical values as follows: $x = m \Delta x$ and $y = n \Delta y$; $j = \sqrt{-1}$

Similarly, the diffuser is numerically written as follows:

$$D(x, y; \lambda) = d(m \Delta x, n \Delta y) \exp[(j) \text{rand}(m \Delta x, n \Delta y; \lambda_i)] \quad (3)$$

Where rand is a random value which is included in the range from 0 to 1, and $d(m \Delta x, n \Delta y)$ is the amplitude weighting factor.

For example, if the image has square dimensions of 2cm height and 2 cm width

and the diffuser has the same dimensions, then $\Delta x = \Delta y = 18 \mu\text{m}$.

The complex amplitude of the Fourier hologram is obtained by operating the FFT upon the multiplication product of the two matrices represented in Eq.2 and Eq.3.

Hence, the complex amplitude of the hologram $B(u, v)$ is represented as follows:

$$\begin{aligned} B(u, v) &= F.T. [A(x, y; \lambda) D(x, y; \lambda)] \\ &= F.T. A(x, y; \lambda) * F.T. D(x, y; \lambda) \xrightarrow{\text{yields}} A_{\text{holo}}(u, v; \lambda) * D_{\text{holo}}(u, v; \lambda) \end{aligned} \quad (4)$$

Where (u, v) are the spatial coordinates in the Fourier plane.

2nd step: Reconstruction Process (Inverse Fourier Transform)

$$\begin{aligned} c(x', y') &= F.T^{-1} [A_{\text{holo}}(u, v) * D_{\text{holo}}(u, v)] \\ &= A_{\text{reconst}}(x', y') \cdot D_{\text{reconst}}(x', y') \end{aligned} \quad (5)$$

Where (x', y') represent the Cartesian coordinates in the imaging plane or the reconstruction plane. The numerical reconstruction images are of maximum dimensions at $x' = x'_{\text{max}} = M \Delta x'$ and $y' = y'_{\text{max}} = N \Delta y'$ for the matrix of dimensions of 1024×1024 pixels.

The Isolation of the Cancer from the Mammographic Image using Segmentation

The following steps are considered for segmentation process:

- 1- Pre-processing using Median filter.
- 2- Determine the connected components.
- 3- Compute the area of each component
- 4- Remove small objects.
- 5- Remove connected objects on border.

The cell of interest has been successfully segmented, but it is not the only object that has been found. Any objects that are connected to the border of the image can be removed using the imclearborder function.

- 6- Interference of the segmented image.

All these operations are executed using Mat-Lab codes.

Segmented Images Modulated by Multiple Beam Interference

The intensity distribution in case of ordinary FPI is given by the formula [31]:

$$I(\delta; R) = \frac{T^4}{1 + R^4 - 2R^2 \cos(\delta)} \quad (6)$$

Where, T is the transmission coefficient while R is the reflection coefficient of the interferometer. δ , is the phase difference between any two adjacent emerging rays.

The equation (6) is used in the modulation of the segmented images.

RESULTS AND DISCUSSION

The input cancerous mammographic image of dimensions 512×512 pixels used in the formation of the coded image is shown as in the figure (1). The Fourier hologram considered for coding the image is fabricated using equation (4) and the Mat- Lab code. The hologram is plotted as in the figure (2). It has dimensions of

1024×1024 pixels. The reconstructed conjugate images obtained from the hologram before filtration, using equation (5), are shown as in the figure (3- a). It is shown, referring to equation (5), that the noise in the reconstructed image is due to the diffuser superimposed over the image. while the same plots of improved image contrast where we get rid of the noise using the Wiener filter are shown as in the figure (3- b).

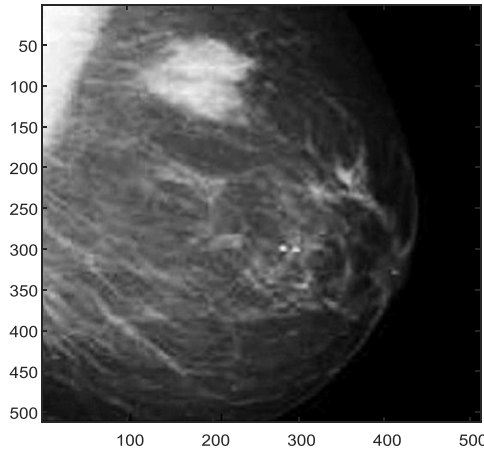


Figure (1): Image of cancerous mammographic image of dimensions 512×512 pixels.

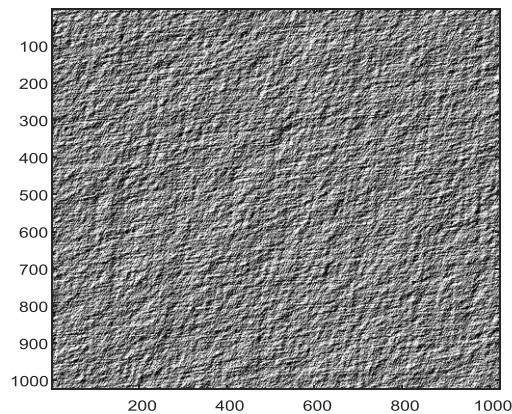


Figure (2): The Fourier hologram of the mammographic image shown in the figure (1). The hologram of the coded image has dimensions of 1024×1024 pixels.

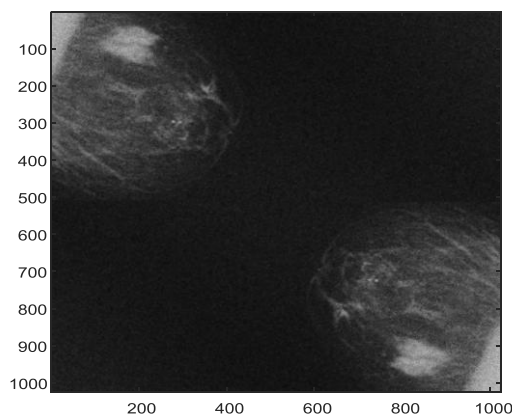


Figure (3- a): Reconstructed conjugate images corresponding to the cancerous mammographic image before filtration. The images are affected by multiplicative noise.

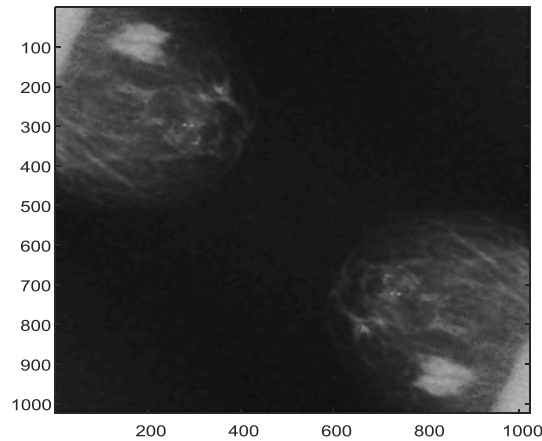


Figure (3- b): Reconstructed conjugate images corresponding to the cancerous mammographic image after filtration. The Wiener filter is used in the filtration of the image.

The input image used for cancer isolation in the segmentation process is again in the figure (1). The Pre- processed image using the Median filter is shown in the figure (4- a). The determination of the connected components in the Pre- processed image is given as in the figure (4- b). The removal of small objects from the connected components in the Pre- processed image is plotted as in the figure (4- c). While the removal of connected objects on the border is shown as in the figure (4- d). The rescaled image after the removal of connected objects on

the border of dimensions 512×512 pixels is given in the figure (4- e). Figure (4- f): The interference fringes modulated by the Black and White (B/W) image is plotted as in the figure (4- f), while that modulated by the mammographic segment is shown as in the figure (4- g). A binary image of the segmented cancer in the mammographic image plotted as in the figure (4- e) while a grayscale image of the cancer is shown in the figure (5). A noise is appeared to the right of the image far from the cancer segment.

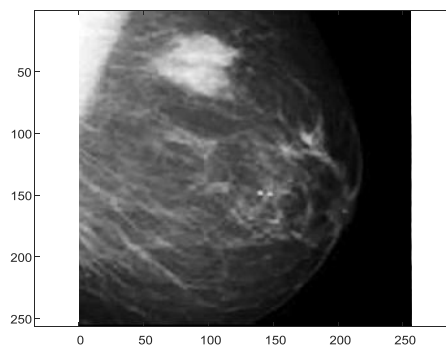


Fig (4- a): Pre- processed cancerous mammographic image using the Median filter.

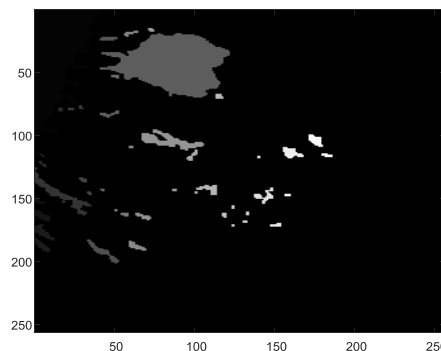


Fig (4- b): Determination of the connected components in the Pre- processed image.

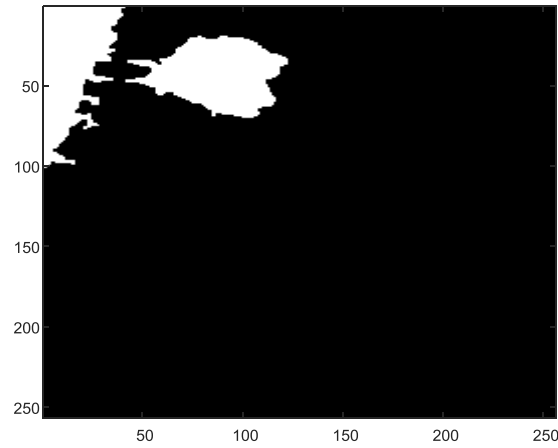


Fig (4- c): Removal of small objects from the connected components in the Pre- processed image.

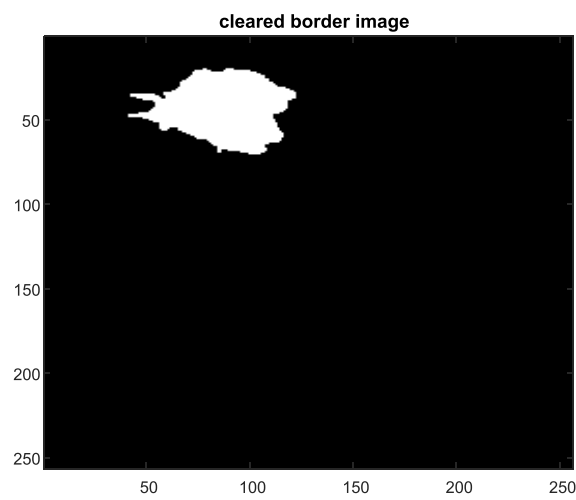


Figure (4- d): Removal of connected objects on the border.

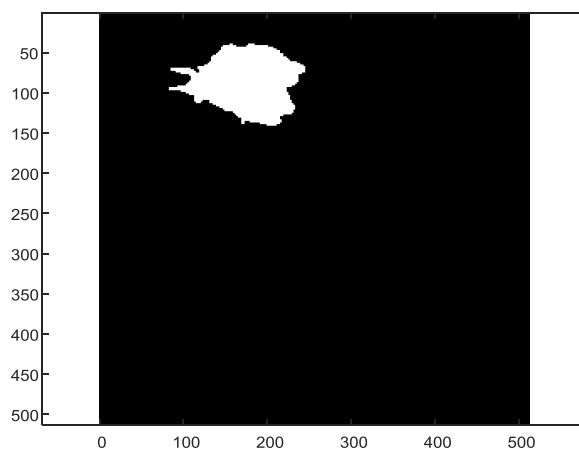


Figure (4- e): The rescaled image after the removal of connected objects on the border of dimensions 512×512 pixels.

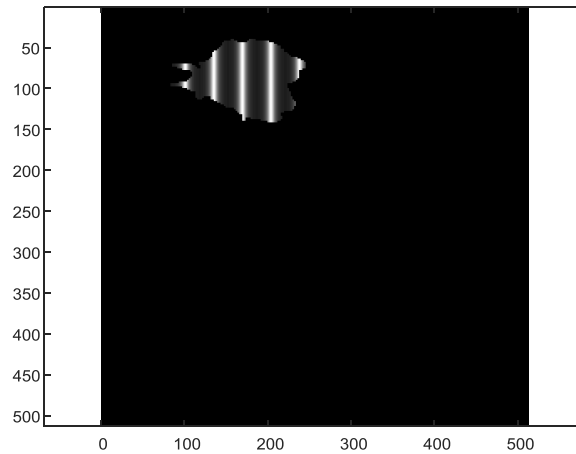


Figure (4- f): The interference fringes modulated by the Black and White (B/W) cancerous segment from the rescaled image of dimensions 512×512 pixels.

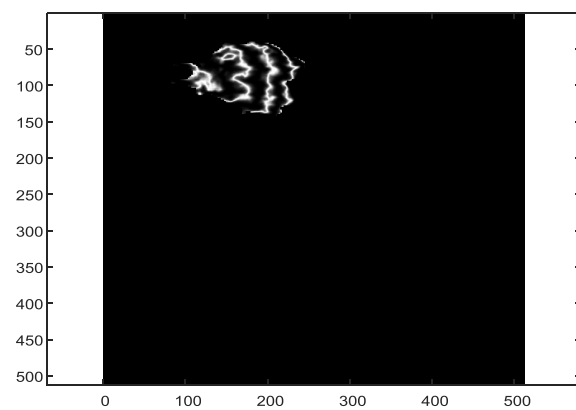


Figure (4- g): The interference fringes modulated by the cancerous segment from the rescaled image of dimensions 512×512 pixels.

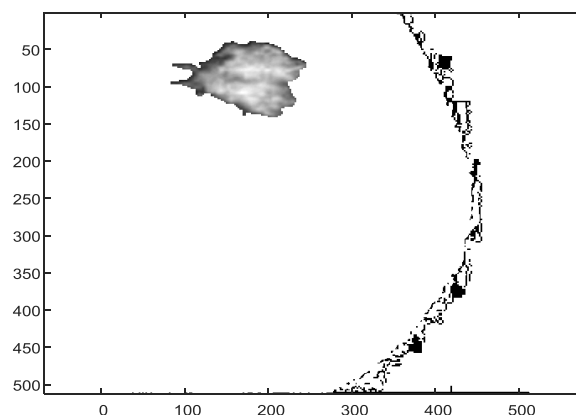


Figure (5): The gray scale image of the isolated segmented cancer in the mammographic image. A noise is appeared, from the computations, to the right of the image.

The line plot of the cancerous segment shown in the figure (4- g) from the rescaled image of dimensions 512×512 pixels is given as in the figure (6). The horizontal range of the segment extends from 103 to 235 pixels while the

vertical range extends from 37 to 137 pixels. Three plots at different vertical sections at 60, 85, and 110 pixels are shown as in the figure (6). The different locations shown in the plots give information about the topography of the

Image Processing of Mammographic Images using Holography and Interferometry

cancer segment as well as its shape. For example, a mid-point located at 165 pixels for two close peaks appeared in the vertical line at

60 pixels, while it is located at 173 pixels for two close peaks corresponding to the vertical line at 85 pixels.

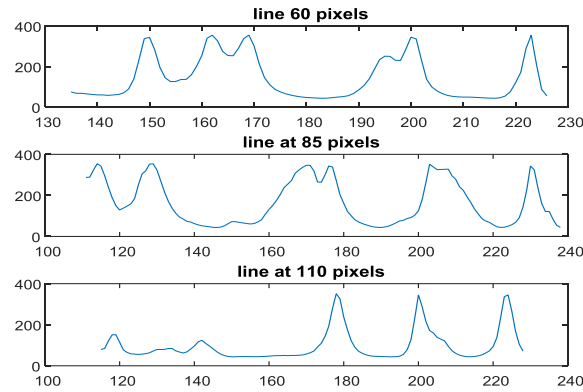


Figure (6): The line plot of the cancerous segment from the interferometric image of dimensions 512×512 pixels. The horizontal range of the segment extends from 103 to 235 pixels while the vertical range extends from 37 to 137 pixels.

Similar procedure for segmentation is applied on the tumor mammographic image as shown in the figure (7). The results of interferometric segmentation are plotted as in the figures (8 a- g). A binary image of the segmented tumor plotted as in the figure (8- e) while a grayscale image of the tumor is shown in the figure (9). The line plots for the segmented tumor in the mammographic image is shown as in the figure (10 a, b).

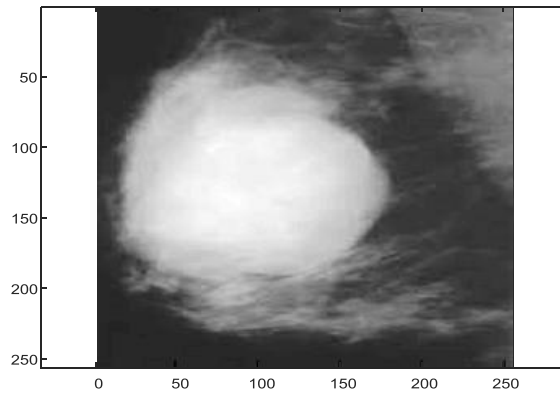


Figure (7): Tumor in the mammographic input image of dimensions 256×256 pixels.

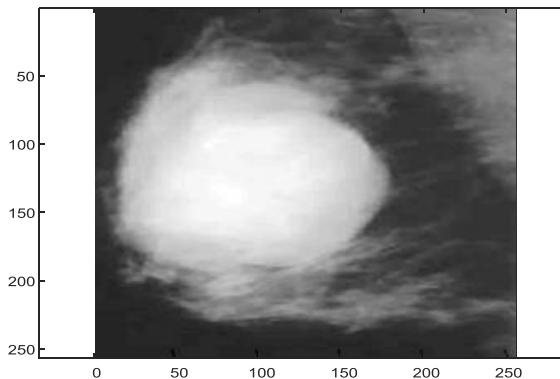


Fig (8- a): Pre- processed tumor image using the Median filter.

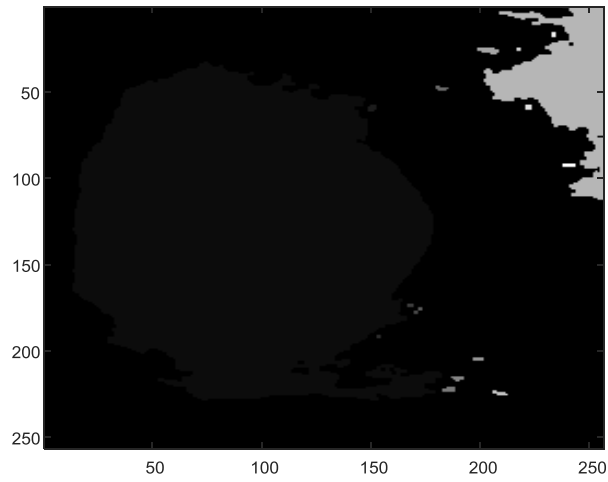


Fig (8- b): Determination of the connected components in the Pre- processed tumor image.

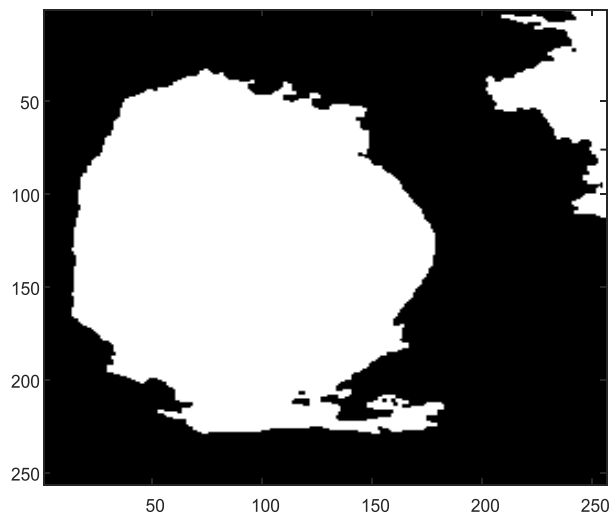


Fig (8- c): Removal of small objects from the connected components in the Pre- processed image.

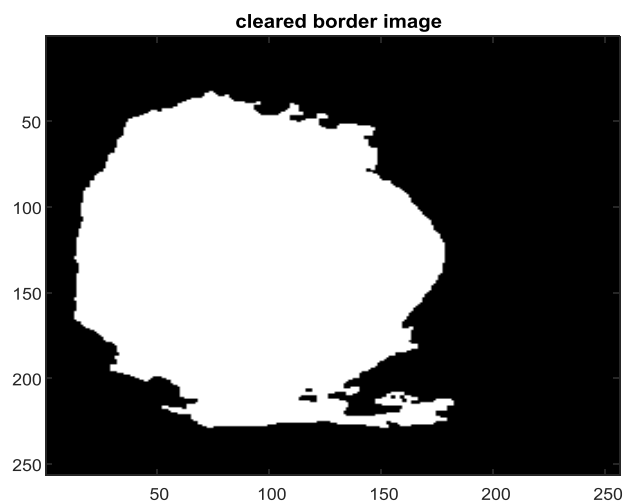


Figure (8- d): Removal of connected objects on the border of the tumor image.

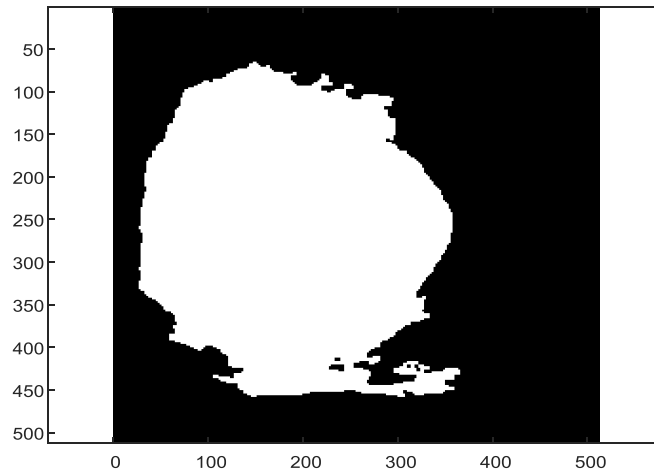


Figure (8- e): The rescaled tumor image after the removal of connected objects on the border of dimensions 512×512 pixels. The reconstructed tumor is binary image $[0,1]$.

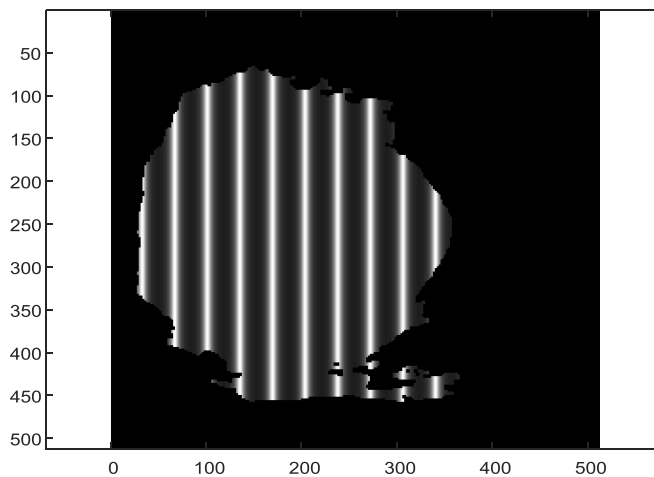


Figure (8- f): The interference fringes modulated by the Black and White (B/W) tumor segment in the image of dimensions 512×512 pixels.

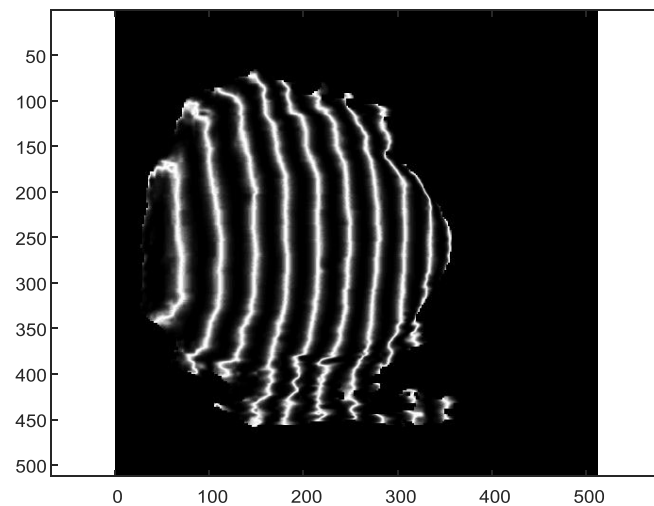


Figure (8- g): The interference fringes modulated by the rescaled tumor segment in the image of dimensions 512×512 pixels.

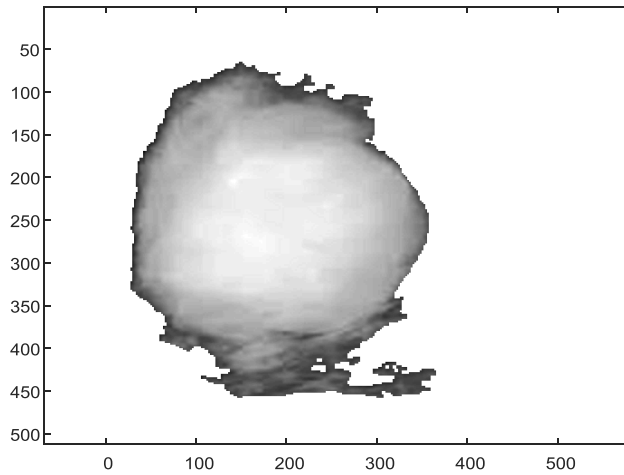


Figure (9): The reconstructed tumor in grayscale image after segmentation.

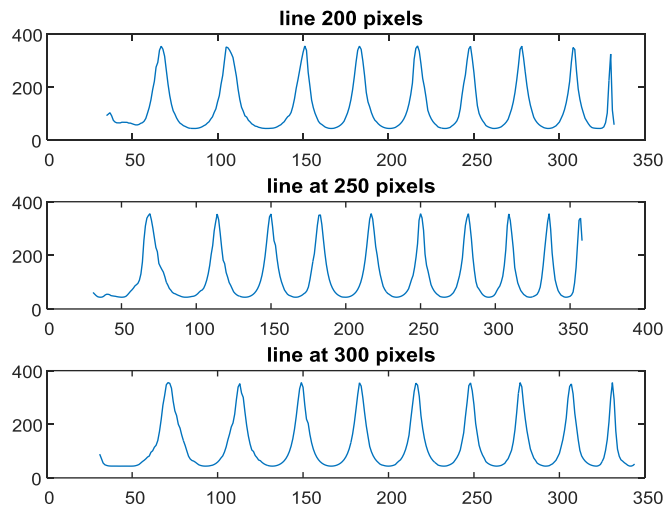


Figure (10- a): The line plot of the tumor segment from the interferometric image of dimensions 512×512 pixels. The tumor is found nearly at the center of the image. The plot at the tumor center at nearly 250 pixels is shown in the middle while the other two plots at 200 and 300 pixels are shifted due to the fringe shift occurred from the tumor image.

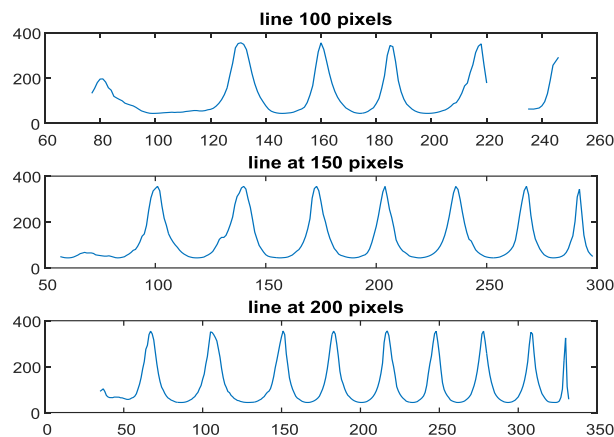


Figure (10- b). The line plot of the tumor segment from the interferometric image of dimensions 512×512 pixels. three plots are shown at 100, 150, and 200 pixels.

Three plots are given at vertical sections at 200, 250, and 300 pixels as shown in the figure (10- a). Another three plots corresponding to the tumor segment at 100, 150, and 200 pixels, as shown in the figure (10- b), are much shifted showing that the fringe shift occurred from the tumor image is at different location. For example, only 4 peaks are shown at 100 pixels while 7, and 9 peaks are located at 150, and 200 pixels respectively. Hence, the maximum tumor width corresponds to the maximum number of peaks as shown in the figure (8- a) for the plots at 200, 250, and 300 pixels.

CONCLUSION

Firstly, we fabricated coded cancerous and tumor mammographic images, without segmentation, using improved Fourier holography.

Secondly, we apply the segmentation procedure and multiple beam interference on the cancerous and tumor images in order to get information about the cancer and tumor shapes from the interferometric segments.

Finally, the tumor and cancer segments are obtained as gray scale image and as interferometric images.

REFERENCES

- [1] M. Agour, C. Falldorf, and C. von Kopylow, *Journal of Optics*, **12** (2010) 1-7, Digital Pre-filtering Approach to Improve Optical Reconstructed Wave fields in Opto -Electronic Holography.
- [2] J.W. Goodman (2005), Introduction to Fourier Optics and Holography. 3rd Edition, Roberts & Company Publishers, Greenwood Village.
- [3] A.M. Hamed, *Optica Applicata*, **X111** (1983) 205-213, Polychromatic Image Processing Using Thick Holographic Multiplexed Filter
- [4] R.N. Bracewell, (1978) Fourier Transform and Its Applications, Chap. 18. McGraw-Hill, New York.
- [5] A.E. Macgregor, *American Journal of Physics* **60** (1992) 839-846, Computer generated holograms from dot matrix and laser printers. <http://dx.doi.org/10.1119/1.17067>
- [6] S. Trester, *American Journal of Physics*, **64**(1996)472-476, Computer Simulated Holography and Computer Generated Holograms. <http://dx.doi.org/10.1119/1.18194>
- [7] G. Pedrini, S. Schedin, and H.J. Tiziani, *Optics Communications*, **171**(1999)29-36, Lensless Digital Holographic Interferometry for Measurement of Large Objects. [http://dx.doi.org/10.1016/S0030-4018\(99\)00486-1](http://dx.doi.org/10.1016/S0030-4018(99)00486-1)
- [8] C. Wagner, S. Seebacher, W. Osten, and W. Jüptner, *Applied Optics*, **38**(1999) 4812-4820, Digital Recording and Numerical Reconstruction of Lensless Fourier Holograms in Optical Metrology. <http://dx.doi.org/10.1364/AO.38.004812>
- [9] A.C. Bovik, and S.T. Acton, (2000) Basic Linear Filtering with Application to Image Enhancement. In: Bovik, A.C., Ed., *Handbook of Image and Video Processing*, Academic Press, San Diego.
- [10] M. Agour, E. Kolenovic, C. Falldorf, and C. von Kopylow, *Journal of Optics A: Pure and Applied Optics*, **11** (2009) Article ID: 105405, Suppression of Higher Diffraction Orders and Intensity Improvement of Optically Reconstructed Holograms from a Spatial Light Modulator. <http://dx.doi.org/10.1088/1464-4258/11/10/105405>
- [11] A.M. Hamed, *Optics and Photonics Journal*, **1** (2011) 52-58, Scanning Holography Using a Modulated Linear Pupil: Simulation. DOI: [10.4236/opj.2011.12008](https://doi.org/10.4236/opj.2011.12008)
- [12] A.M. Hamed, *Optics and Photonics Journal*, **4**(2014) 136-142, Holographic imaging of Argon plasma images. DOI: [10.4236/opj.2014.46014](https://doi.org/10.4236/opj.2014.46014)
- [13] N Barakat and S Mokhtar, *J. Opt. Soc. Am.*, **53**(1963)300- 301, On the factors contributing to the formation of multiple beam Fizeau fringes.
- [14] N Barakat and A M Hindelah, *Textile Res. J.*, **41**(1964) 581- 584, Determination of the refractive indices, birefringence, and tensile properties of normal viscose rayon fibers.
- [15] N Barakat, "Interferometric studies on Fibers: Part I: Theory of interferometric determination of Indices of Fibers", *Textile Res. J.*, vol. **41**, pp. 167, 1971.
- [16] M M El Nicklawy and I M Fouda, "An analysis of Fizeau fringes crossing a fiber with a multiple skin", *Textile Res. J.*, vol. **71**, pp. 252- 256, 1980.
- [17] A Hamza, T Z N Sokkar and M A Abeel, "Interferometric determination of optical properties of fibers of irregular transverse section and having a skin- core structure", *J. Phys. D*, vol. **18**, pp.1773 1985.
- [18] A Hamza, T Z N Sokkar and M A Abeel, "Interferometric determination of refractive indices and birefringence of fibers with irregular transverse sections", *J. Phys. D* vol. **19**, pp. 119 , 1986.
- [19] N. Barakat, A Hamza and A Goned, "Multiple beam interference fringes applied to GRIN optical waveguides to determine fiber characteristics", *Appl. Opt.*, vol. **24**, pp. 4383- 4386, 1985.
- [20] L M Boggs, H M Presby and D Marcuse, "Rapid automatic index profiling of whole fiber samples: part I" *Bell System Tech. J.*, vol. **58**, pp.867- 882, 1979.
- [21] H M Presby, D Marcuse, H W Astle and L M Boggs, "Rapid automatic index profiling of whole

- fiber samples: part II”, Bell System Tech. J., vol. **58**, pp. 883- 902, 1979.
- [22] A. M Hamed, “Fourier imaging of un-cladded fibers using a liquid wedge interferometer”, Opt. Appl. Vol. **xxvii**, pp.229- 240, 1997.
- [23] A. M Hamed, “Modeling of the fringe shift in multiple beam interference for glass fibers”, Pramana – J. Phys., vol. **70**, pp. 643- 648, 2008.
- [24] N Barakat and A Hamza, Interferometry of fibrous materials (Bristol, Adam Hilger, Ltd. Techno House, 1990)
- [25] M Born and E Wolf, Principles of Optics, 2nd ed., Pergamon Press Ltd., Oxford (1964) page 328.
- [26] A.M. Hamed, Some applications of scattered light and multiple beam interference using coherent light, M.Sc. Thesis, 1976.
- [27] A. M Hamed, “Investigation of SIDA virus (HIV) images using interferometry and speckle techniques”, Int. J. Innovative Res. in Comp. Sci. and Tech. (IJRCST),vol. 4, pp.38- 45, 2016.
- [28] A. M Hamed, “Image processing of corona virus using interferometry”, Optics and Photonics Journal, vol. 6, pp. 75 – 86, 2016.
- [29] A.M. Hamed, Topics on optical and digital image processing using holography and speckle techniques, publisher by Lulu.com, ISBN 9781329328464 Nov. 29, 2015.
- [30] A.M. Hamed, Int. J. Photonics and Optical Technology, 3(2017)67- 71, A modified Michelson interferometer and an application on microscopic imaging.
- [31] A. M. Hamed, www.lap.com (Lambert Academic Publishing), 14 Nov. (2017), The Point Spread Function of some modulated apertures (Application on speckle and interferometry images) ISBN:9786202070706.

Citation: A.M. Hamed, “Image Processing of Mammographic Images using Holography and Interferometry”, *International Journal of Emerging Engineering Research and Technology*, 7(12), pp.1-12.

Copyright: © 2019 A.M. Hamed. This is an open-access article distributed under the terms of the Creative Commons Attribution License, which permits unrestricted use, distribution, and reproduction in any medium, provided the original author and source are credited.